IEEE Access
Multidisciplinary | Rapid Review | Open Access Journal

Received July 20, 2019, accepted August 10, 2019, date of publication August 19, 2019, date of current version August 31, 2019.

Digital Object Identifier 10.1109/ACCESS.2019.2936132

Sensitivity Analysis and Classification Algorithms Comparison for Underground Target Detection

SHIHONG DUAN[1], YUE LI[1], YADONG WAN[1], PENG WANG[1,2], ZHEN WANG[1], AND NA LI[3]

[1]School of Computer and Communication Engineering, University of Science and Technology Beijing, Beijing 100083, China
[2]Sunkaisens (Beijing) Technology, Ltd., Beijing 100071, China
[3]School of Mathematics and Physics, University of Science and Technology Beijing, Beijing 100083, China

Corresponding authors: Yadong Wan (wyd@ustb.edu.cn) and Peng Wang (wangpeng.micl@gmail.com)

This work was supported in part by the China Postdoctoral Science Foundation under Grant 2019M650778, in part by the Fundamental Research Funds for the Central Universities under Grant 2302018FRF-GF-18-016B, and in part by the National Natural Science Foundation of China (NSFC) under Project 61671056.

ABSTRACT Underground target detection technology has been widely used in urban construction and resource exploration. With the development of industrial modernization, the demand for underground target detection is becoming more specific, such as the material and shape of underground targets. Therefore, it is necessary to classify the properties of underground targets. In this paper, sensitivity analysis was performed on the spheroid model and the approximate forward model at first, and the influence of the target properties on the model output is obtained. Secondly, we utilized the fitting algorithm to obtain the model parameters of the simulation data (model response of targets with varying shapes and materials), and analyzed the influence of the fitting algorithm on the classification results at different SNR. Finally, eight machine learning algorithms: support vector machine(SVM), neural network(NN), quadratic discriminant analysis (QDA), Gaussian process (GP), decision tree (DT), random forest (RF) and AdaBoost were used in this study to compare the obtained results. From the above analysis, we found that the shape (radius) have a greater influence on the model than the material (permeability) in the spheroid model. According to the approximate forward model, we found that it is not feasible to classify targets when the orientation is unknown. The influence of the fitting algorithm on the classification performances is related to the noise level. The obtained results using neural network demonstrated that the proposed method outperformed in material-based classification and shape-based classification. In the material-based classification, the classifier generally has a weaker ability to distinguish between permeable materials.

INDEX TERMS Underground target detection, sensitivity analysis, fitting algorithm, machine learning, classification algorithms comparison.

I. INTRODUCTION

With the development of industrial modernization, metal target detection technology plays an important role in some important fields, such as security [1], transportation [2], historical humanities [3], engineering construction [4], resource exploration [5], and so on. In the above-ground detection, metal detection technology is mature and has been widely used in security(for example, in the security inspection to eliminate dangerous goods [6]), which has played an important role in promoting the development of security check. In the case of underground exploration, metal detection technology has been used in historical humanities (e.g. archaeological treasure hunting [7]), transportation (e.g. highway subgrade detection [8]), urban construction (e.g. detection of urban underground metal pipelines [9]), engineering construction (e.g. geological mapping [10]), and resources exploration (e.g. mineral exploration [11]).

At present, the underground metal targets detection based on electromagnetic eddy current method has become a mature technology, which achieves the purpose of detecting targets by acquiring the eddy current induced by the target object in a changing magnetic field [12]. Because of its high sensitivity to metal materials, high precision, and strong penetrability,

The associate editor coordinating the review of this article and approving it for publication was Najah Abuali.

the electromagnetic detection method is suitable for target detection in complex underground environments [13].

The electromagnetic metal detector is based on the principle of electromagnetic induction and generates a variable magnetic field with alternating current in the coil. Metal objects are affected by the variable magnetic field and produce induced eddy current, which generates a induced magnetic field [14]. The interaction between the induced magnetic field and the original magnetic field triggers the sound of detector, reporting the existence of metal objects to users (e.g. security inspectors [15], treasure seekers, archaeologists [16]). For above-ground target detection, reporting the existence of metal objects can meet the needs of the most practical applications. However, only existence information cannot meet the needs of underground target detection. Taking engineering construction as an example, we need to know the distribution of underground metal pipelines before building public service facilities. Due to the lack of reasonable planning in early urban construction, the limited level of municipal management, and the lack of effective archival data management, there is no systematic record of underground pipeline distribution, pipeline material and pipeline shape [17]. With the development of industrial construction, underground pipelines are all over the city [18]. Only by obtaining the location information, specific material and shape of the underground pipelines, we can smoothly carry out the construction of the projects. Therefore, distinguishing the material and shape of the target based on the detected information becomes an urgent problem to be solved, that is, the classification problem.

At present, the research on the classification for underground metal targets mainly focuses on two aspects: model based methods and data based methods. The classification process of the two methods is shown in the top half of Fig. 1. For the model based method, a model is established based on the magnetic field attenuation response of the target object, and then the material and shape are classified by the model parameters. The classical response model of magnetic field attenuation is proposed in [19]. Smith *et al.* improved the fitting effect on the early response for the permeable sphere and proposed a more mature attenuation response model [20]. In terms of classification, Pasion *et al.* conducted a detailed study on the relationship between the parameters in the model of the axi-symmetric metal object and the properties of the target object, and proposed a method of using model parameters as indicators of classification [21]. For the data based method, the classification of the target object is achieved by analyzing the magnetic field attenuation response value of the target object. However, not all the attenuation response data contribute to the classification, and the useful data need to be selected carefully. In [22], the optimal magnetic susceptibility characteristics were determined by the Relevant Vector Machine (RVM) feature selection method, and weights were assigned. In terms of classification, the classification threshold is estimated by performing a principled Bayesian risk analysis on the magnetic susceptibility characteristics to achieve the purpose of classifying the underground targets.

The ultimate purpose of categorizing the target is to improve classification accuracy. The current research focus is generally to classify the target by analyzing the parameters in the object response model or the target attenuation response value. In general, the researches is to improve the classification effect of the target, but most of them are promoting at a certain point in the classification system to achieve better classification results. In order to provide a systematic idea for improving the classification effect, we have analyzed the whole classification system in this paper, and summarized and analyzed the factors that may affect the classification results in the classification process as well.

The main research content of this paper is to classify the material and shape of the target by analyzing parameters of the magnetic field attenuation response model of the target object. The classification process is shown in the lower part of Fig.1. On this basis, the factors affecting the classification results in the whole classification process were analyzed.

Firstly, the sensitivity analysis was performed on the ellipsoid model and the approximate forward model. For the spheroid model, we evaluated the relationship between the properties (shape and material) of the target object and the model parameters. The simulation results show that in the sensitivity analysis of the spheroid model, the target radius has a greater influence on the model parameters than the target material. In the case of the model parameters as the classification feature, the results exhibits that the classification results of the target shape is better than that of the target material. For the approximate forward model, we evaluated the influence of target object's properties and orientation on the model parameters. In the sensitivity analysis of the approximate forward model, the influence of the target orientation on the model parameters is unfixed. In some cases, influence of the target orientation is much greater than that of other parameters. To achieve a better classification results, obtaining object orientation information before classification is necessary. It is not feasible to classify targets when the orientation is unknown.

Secondly, in order to be closed to the real situation, we have added different noise to the simulation data and obtained the model parameters by fitting algorithm. We used the model parameters as classification features to classify the properties of object. By comparing the classification results, we can obtained the influence level of the fitting algorithm on the classification results at different SNR. By studying the influence of the fitting algorithm on classification, fitting algorithm has different influences on classification results at different SNR. As the SNR increases, we found that the classification results of the fitted data get better. The results of the fitting algorithm are very sensitive to the noise level.

Finally, we used the model parameters as classification features, inputted them into a variety of machine learning algorithms and obtained the classification results. By comparing the classification results with different evaluation metrics,

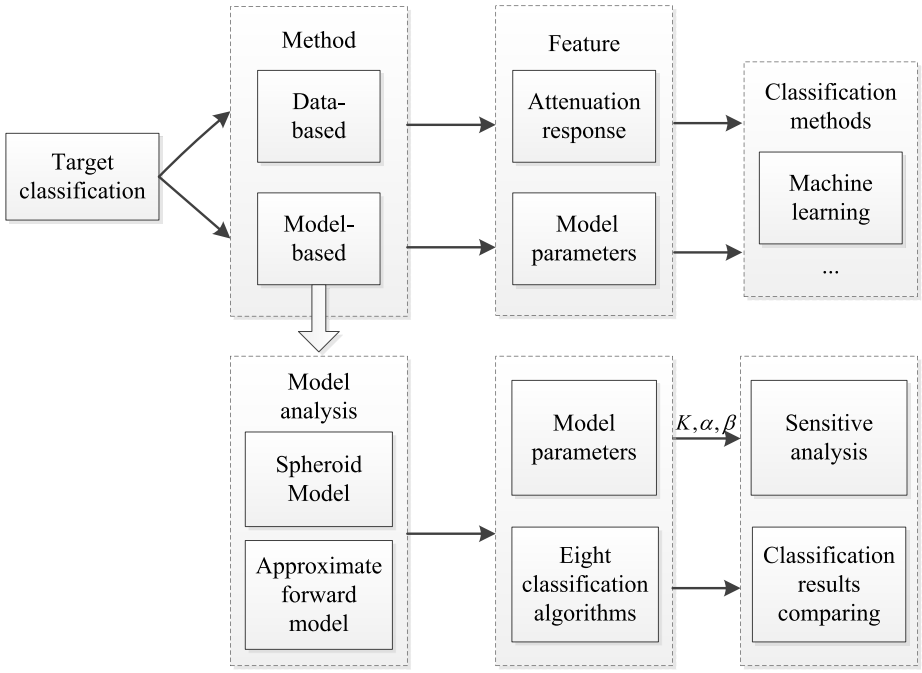

FIGURE 1. The classification process of the model-based method and data-based method.

we got the influence of different classifiers on the classification performances. By studying the impact of classification algorithms on classification, we compared the influences of different classifiers with multiple classification algorithm evaluation metrics. The results show that most classifiers have a weaker ability to distinguish permeable materials in material-based classification. Overall, most classifiers have a stronger ability to distinguish object shapes than object materials. In addition, the neural network has a good performance in the material-based classification and shape-based classification.

The innovations of this paper are as follows:

A. *Sensitivity analysis is used to evaluate the influences of object properties (shape, material) on model parameters in the spheroid model.*
B. *Sensitivity analysis is used to evaluate the influences of object property (shape) and orientation on model parameters in the approximate forward model.*
C. *From the perspective of classification label (material-based classification and shape-based classification), the influence of noise on the fitted parameters and the influence of the fitting algorithm are analyzed.*
D. *The classification performance of eight machine learning algorithms is compared by the analysis of the recall rate, precision and confusion matrix.*

The details of this paper are arranged as follows. In the second section, the spheroid model, approximate forward model and sensitivity analysis are introduced. In the third section, we introduce the machine learning classification algorithm and the common classification metrics. In the fourth section, the factors affecting the classification performance are analyzed in the whole classification process. In the fifth section, we summarizes the article to give conclusions and directions in future work.

II. RELATED WORK

The classification of underground targets is carried out by obtaining the electromagnetic characteristics of the target from the acquired magnetic field data and analyzing the physical characteristic parameters of the target, thereby distinguishing the target of interest from other objects and reducing the false-alarm counts [23].

There are two main types of parameters used for classification: data-based parameters, which can be obtained directly from magnetic field data, such as the amplitude [24], induction data [25] etc. Model-based parameters, generally electromagnetic propagating parameters of the forward model, such as dipole models, ortho-normalized volume magnetic source (onvms) models [26], etc.

Data-based parameters and model-based parameters can be used as input to statistical classification methods. These parameters are related to the physical characteristics of the target, and the classification results can be used as a basis for determining whether the target is the target of interest. The frequently used data classification methods include support vector machine (SVM) [27],random forest [27], neural network [27], [28], k-neighbor [24] and unsupervised weighted-pair group method with averaging (WPGMA) algorithm [26].

Recently, many researchers reported the classification of underground targets by model-based parameters

and data-based parameters. In model-based classification, Bijamov *et al.* utilized combined clustering/Gaussian-mixture-model approach to generate the training list and evaluated the likelihood of an object being a UXO by the list. The model parameters are corrected iteratively through the ground truth, so that all targets of interest can be identified correctly [29]. Bray and Link utilized FEM model response and actual TFM field data as training data in discrimination and classification approaches, and compared the classification performance of neural networks, random forests, and support vector machines [27]. In [25], the detailed steps of UXO classification procedure using the advanced EMI sensors and models are presented along with the processing and analysis approaches that are used to generate a prioritized dig list. Makkonen *et al.* classified the inversion results of magnetic polarizability tensor by comparing the library data and K-nearest neighbor classification algorithm to determine the class of targets [24]. Sigman *et al.* utilized target extrinsic and intrinsic parameters as data set. (dimensionality reduction by Pasion-Oldenburg model) and cluster the anomalies by unsupervised weighted-pair group method with averaging (WPGMA) algorithm. A supervised Gaussian mixture model (GMM) is trained for each cluster [26], (in which each class of UXO is represented by a multivariate Gaussian probability density.)

For data-based classification, In [30], authors combined the method of ''voting by comparing the polarizability with the library data'' and the method of ''Bayesian statistics on features extracted from the polarizabilities'' to generates an ordered dig list. Mitiche *et al.* mapped time-domain signal to a Bispectrum image and classified the high-pressure discharge signals by using a deep residual neural network to classify the Bispectrum images [31]. Ammari *et al.* identified conductive objects by extracting geometric features from the induction data and matching the features data for known objects from a given dictionary [14]. In [28], the convolutional neural network (CNN) is capable of recognizing whether a B-scan profile obtained from ground-penetrating radar (GPR) acquisitions contains traces of buried mines. Kanafiah *et al.* utilized the amplitude peak, skewness and standard deviation values of the hyperbolic signal obtained by GPR detection as the classification feature and utilized the multilayer perceptron (MLP) learning algorithm to classify the shapes which are a metal cube and metal cylinder [32].

The related works classified the target by using specific data sets or matching the features from library data, but most of them only promoted at a certain point in the classification system to achieve better classification results. This means that the quality of the classification results depends on the authors 'expertise and specific data sets [33], and the method of improving the classification results is more targeted. In order to find a general method to improve the classification results, we have analyzed the whole classification system in this paper and analyzed the factors that may affect the classification results in the classification process as well.

III. SYSTEM MODEL

In the detection system, the metal target is located at a certain position in the underground space. When primary field (generated by transmitter) acts on the metal target, secondary field is generated by the eddy current of metal target. The secondary field data are collected by the detector sequentially placed in different positions on the detection plane. Estimation of the target's parameters can be obtained from these secondary field data.

The geographical condition we refer to is the land where metal targets and clutters are buried underground. It is located in Aberdeen Maryland and Yuma Arizona.

In this paper, the purpose of the classification is to correctly distinguish the material of the underground target. We can divide materials into permeable materials and non-permeable materials. Take the detection of underground pipelines as an example, most of the underground pipelines are permeable materials (relative permeability > 1), so we chose the representative permeable material nickel (relative permeability $= 99.47183638$) and steel (relative permeability $= 696.3028547$) as the materials to be classified. The materials of other clutter are mostly non-permeable materials (relative permeability ≈ 1), so we chose the non-permeable material aluminum as the materials to be classified.

In order to obtain the better classification results of the target properties, we need to model the relationship between the magnetic field response and the target parameters. There are three models are discussed in this section: general model; spheroid model and the approximate forward model. The general model is a model that is adaptable to objects of any shape. The spheroid model is a model suitable for axi-symmetric objects. In this paper, the spheroid is utilized as the main research object to model the polarization tensor $L(t)$ .The approximate forward model is a model close to the real measurement scene, it considers the orientation of the underground buried object based on the spheroid model.

A. GENERAL MODEL

Assuming the conducting object is illuminated by a uniform primary field, when the primary field is terminated, the eddy current will induced in the object. Finite conductivity of an object leads to current decay, the secondary field $B^S(t)$ (Fig. 2) produced by decaying current is dipolar:

$$B^S(t) = \frac{\mu_0}{4\pi r^3}\vec{m}(t) \cdot \left(3\hat{r}\hat{r} - \bar{\bar{I}}\right) \tag{1}$$

where μ_0 is the vacuum permeability, $\vec{m}(t)$ is the induced dipole moment at the center of the object at time t, r is the distance from the observation point to the center of the object, and $\hat{r}$ is the unit vector from the center of the object to observation point, $\bar{\bar{I}}$ is the identity dyadic [21].

The induced dipole moment is generated by the primary field and its value is linearly related to the primary field:

$$\vec{m}(t) = \frac{2\pi}{\mu_0} B^P L^B(t) \tag{2}$$

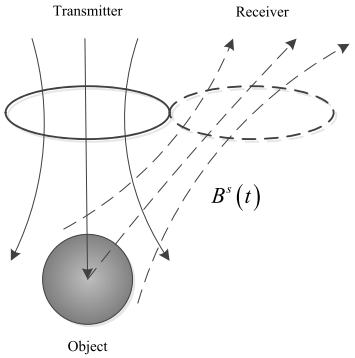

FIGURE 2. Object generates a secondary field $B^S(t)$. Transmitter is the transmitting magnetic field coil. Receiver is the coil that accepts a secondary magnetic field response.

$L^B(t)$ is the time decay response of the object [34], and B^P is the primary field. For convenience, we write the relationship between the induced dipole moment and the primary field as:

$$\vec{m}(t) = \overline{\overline{M}} \cdot B^P \tag{3}$$

The secondary field strength induced by object is as same as the magnetic field strength of the magnetic dipole that located at the object center. For an object of any shape, the secondary response is the sum of the responses of the three orthogonal dipoles [34]:

$$\vec{m} = \vec{m}_1 + \vec{m}_2 + \vec{m}_3 = \overline{\overline{M}} \cdot B^P \tag{4}$$

The strength of the three induced dipole are proportional to the product of the primary field along each of three principal axes and the polarizability. $\overline{\overline{M}}$ is further expressed as [34], [35]:

$$\overline{\overline{M}} = \begin{pmatrix} L_1(t) & 0 & 0 \\ 0 & L_2(t) & 0 \\ 0 & 0 & L_3(t) \end{pmatrix} \tag{5}$$

The primary field has three orthogonal directions, and the three polarization tensor $L_*(t)$ represent the response of the orthogonal axis of the object in parallel with the direction of the primary field, which contains all the information of the object decaying with time, and depends on the material, shape, and size of the object. Polarization tensor play an important role in object classification.

The above is a brief introduction to the general model. The general model is suitable for an object of any shape [34], but in reality most of the target objects we want to distinguish are axi-symmetric objects, such as ellipsoids, cylinders, etc. We can model the axi-symmetric objects based on the general model.

B. SPHEROID MODEL

The response of the metal target in any direction is a linear combination of the responses of each orthogonal axe. If the radius of the three orthogonal axes of the general object are different from each other, the responses in the three directions are different. Therefore, it is necessary to form the general model with three induced dipole moments; for the regular axi-symmetric object, only the transverse radius and the axis radius is different, so it can be represented in the form of two induced dipoles, as shown in Fig.3:

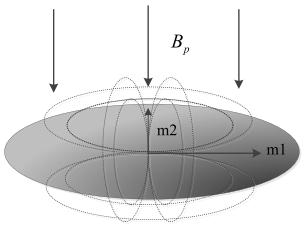

FIGURE 3. Induced dipoles in different orthogonal axes of axi-symmetric objects.

$$\vec{m} = \vec{m}_1 + \vec{m}_2 = \overline{\overline{M}} \cdot B^P \tag{6}$$

The induced dipole $\vec{m}_1$ is parallel to the major axis of the axi-symmetric object, and $\vec{m}_2$ is perpendicular to the major axis of the axi-symmetric object. The strength of the two induced dipoles are proportional to the product of the primary field along the dipole direction and the polarizability [34]. Further, we write the magnetic polarization matrix of the axi-symmetric object in the form of the magnetic polarization tensor:

$$\overline{\overline{M}} = \begin{pmatrix} L_2(t) & 0 & 0 \\ 0 & L_2(t) & 0 \\ 0 & 0 & L_1(t) \end{pmatrix} \tag{7}$$

The magnetic polarization tensor reflects the time decay response of the object, and dipoles in different directions decay independently of each other. For general consideration, we use the spheroid model as the main basis for building the forward model, and magnetic polarization tensor as the parameters related to a target material, shape and so on. Therefore, a more accurate parametric estimation to the magnetic polarization tensor is very important to establishment of the model.

The permeable object of arbitrary shape and size is excited by the main field to generate induced magnetic field, and the decay of induced magnetic field over time is determined by the superposition of the exponents (Kaufman, 1994). Furthermore, the time-domain impulse response of an axi-symmetric object can also be described as the infinity and superposition of the exponents [34].

$$\begin{aligned} L_1(t) &= m_1(0)\,\delta(t) + \frac{\partial}{\partial t}\sum_k u(t)\, m_{1k} \exp(-\omega_{1k} t) \\ L_2(t) &= m_2(0)\,\delta(t) + \frac{\partial}{\partial t}\sum_k u(t)\, m_{2k} \exp(-\omega_{2k} t) \end{aligned} \tag{8}$$

The polarization tensor L_1 reflects the decay information parallel to the major axis of the axi-symmetric object, and L_2 reflects the decay information perpendicular to the major axis of the axi-symmetric object. We can utilize the above formula to parameterize $L_*(t)$, but the parameterization process may be too complicated due to too many parameters. So we should

try to use a functional form that can be defined by a minimum number of parameters and can reflect all the features of the object decay responds over time:

$$f(t) = k\left(1 + \frac{t^{1/2}}{\alpha^{1/2}}\right)^{-\beta} e^{-t/\gamma} \tag{9}$$

As shown in (9), the decay response of object is described as three stages: early time stage, intermediate time stage and late time stage [34], [36]. At the early time stage, the time derivative of the permeable sphere's response to the step function excitation decays as $t^{-1/2}$ [36], and the parameter α describes the transition time from early decay to intermediate exponential decay. The linear decrease in response observed during the intermediate time stage is related to $t^{-\beta/2}$. The exponential decay characterizing the late time stage is related to the parameter γ. Parameter K corresponds to the difference between high frequency and low frequency limit responses [20]. A detailed description of the parameters is given in [20], [36].

A majority of the objects can be approximated as spheroids, and the axial and transverse responses of the spheroid can be approximated as spheres response [37]. Therefore, the magnetic polarization model of the spheroid object in different directions can be expressed as [38]:

$$\begin{aligned} L_n(t) &= \frac{2a^2 b}{9{R_n}^3}\frac{\mu_r+2}{\mu_r}\left[\frac{1}{1-A_n} + \frac{\mu_r-1}{1+A_n(\mu_r-1)}\right] L(t, R_n) \\ R_1 &= b \quad R_2 = a \end{aligned} \tag{10}$$

where μ_0 is the vacuum permeability. R_1 and R_2 correspond to the polar radius b of the spheroid axis and the equatorial radius a of the spheroid transverse respectively. $L(t, R_n)$ is the decay response when the sphere radius is R_1 or R_2. Since the ratio $\rho = a/b$ of the spheroid is unfixed, the demagnetization factor A_n on the different axes will also change. The description of A_n is given in [37].

The decay curve model of the spheroid polarizability and the detailed description of the parameters are introduced. According to the above background, we can write the approximate expression of the secondary field response of the axi-symmetric target, but in reality, due to the orientation of the spheroid is uncertain, so we need to further improve the spheroid model to make it more close to the reality, and then make a more accurate simulation. Next we will introduce the approximate forward model.

C. THE APPROXIMATE FORWARD MODEL

In a real measurement scene, the coordinate system of the transmitter that generated the primary field is generally not the same as that of the target (Fig.4), so in general, the target response in the target coordinate system can be obtained by coordinate transformation:

$$M = U\overline{\overline{M}}\,U^T \tag{11}$$

where $\overline{\overline{M}}$ is the magnetic polarizability tensor matrix of the target, U is the transformation matrix between the observation coordinate system and the metal target coordinate system

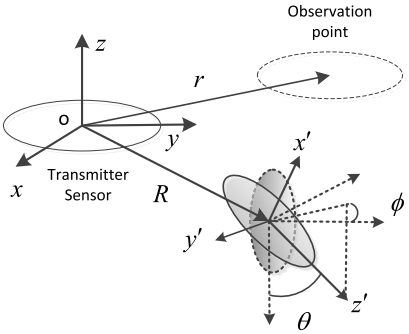

FIGURE 4. The approximate forward model in a real measurement scene, where x, y and z define the coordinate system of the primary field, x', y' and z' define the coordinate system of the target buried underground, and the graph outlined by the dashed line is the target after the coordinate transformation.

(Euler rotation tensor), which can convert the vector in the observation coordinate system into vector in the target coordinate system. The form is as shown in [34]. ψ, θ, and ϕ are the heading angle, pitching angle, and roll angle respectively, but when the target is an axi-symmetric target, the change of the heading angle does not affect the coordinate transformation. For the convenience of calculation, we set $\psi = 0$, at this time, the Euler rotation tensor is:

$$U = \begin{bmatrix} \sin\theta & 0 & -\sin\theta \\ \sin\theta\sin\phi & \cos\phi & \cos\theta\sin\phi \\ \sin\theta\cos\phi & -\sin\phi & \cos\theta\cos\phi \end{bmatrix} \tag{12}$$

The forward model of the spheroid can be expressed as:

$$M = U\overline{\overline{M}}\,U^T = U \cdot \begin{bmatrix} L_2(t) & 0 & 0 \\ 0 & L_2(t) & 0 \\ 0 & 0 & L_1(t) \end{bmatrix} \cdot U^T \tag{13}$$

Thus, the response of the spheroid in the real scene illuminated by the transmitter can be approximated as equation (13). In order to obtain the better classification result, we need to know the important parameters of the target, such as the relationship between model parameters and shape or material, and then analyze the influence of different parameters on the classification results. In the next section, we focus on the analysis of the target properties affect on the model parameters.

IV. SENSITIVITY ANALYSIS

The model parameters are related to the properties of the target. It is necessary to profoundly understand about the influence of the target properties on the model parameters. First of all, although the model parameters can be classified as classification features in intuitive, they have not been verified by theory, thus the classification feasibility cannot be predicted. Secondly, the influence of target properties on several model parameters is not the same. It is necessary to understand the relationship between model parameters and target properties in order to improve the classification results.

We can analyze the relationship between model parameters and target properties by sensitivity analysis. Sensitivity

analysis, as a basic component of complex system analysis, is basically concerned with quantifying the effects of different parameters on the model output. It assists us to identify which parameters in the model are quite essential and which parameters can be neglected, and to deeply comprehend the relationship between input parameters and output variables.

The differential-based method in sensitivity analysis primarily quantifies the significance of the input parameters to the model output based on the differentiation of the input variables from the output variables. Because of its high computational efficiency, and as long as the function expression between the output variable and the input parameter is given, the sensitivity of the output variable in different input parameters can be effectively analyzed, so it is widely used in sensitivity analysis.

The sensitivity analysis of the multi-variable model is described in detail in [39]. The sensitivity analysis of two-variable model is carried out in this paper. First-order Taylor expansion is performed on the model function, and the output variance $V(y)$ is expressed as:

$$V(y) = V(x_1)\left(\frac{\partial f}{\partial x_1}\right)^2 + V(x_2)\left(\frac{\partial f}{\partial x_2}\right)^2 + V(x_1)V(x_2)\left(\frac{\partial^2 f}{\partial x_1 \partial x_2}\right)^2 (\{E\}) \quad (14)$$

where $(\{E\}) = (E_1, E_2)$ represents the mathematical expectation of different input variables at their center point, $V(x_*)$ represents the variance of different input variables, and $V(y)$ can be further decomposed into sub-variance of different dimensions:

$$V_1 = V(x_1)\left(\frac{\partial f}{\partial x_1}\right)^2, \quad V_2 = V(x_2)\left(\frac{\partial f}{\partial x_2}\right)^2 \quad (15)$$

$$V_{12} = V(x_1)V(x_2)\left(\frac{\partial^2 f}{\partial x_1 \partial x_2}\right)^2 \quad (16)$$

V_i represents the contribution of a single variable to output uncertainty, and V_{ij} represents the contribution of the interactions between the variables to output uncertainty. In the sensitivity analysis results, we need to use the measures of sensitivity S_* to quantify the importance of each variables in determining the output uncertainty y. The measures of sensitivity are defined as:

$$S_1 = \frac{V_1}{V(y)}, \quad S_2 = \frac{V_2}{V(y)}, \quad S_{12} = \frac{V_{12}}{V(y)} \quad (17)$$

V. CLASSIFICATION ALGORITHM AND METRICS

According to the current research status, the underground target classification algorithms can be roughly divided into three categories: supervised classification algorithm [40], [41], unsupervised classification algorithm and semi-supervised algorithm [42]. Typical algorithms in the supervised classification algorithm include neural network, support vector machine(SVM), boosting, naïve bayes algorithm and decision tree, etc. The most common algorithm utilized in unsupervised classification algorithm is cluster analysis.

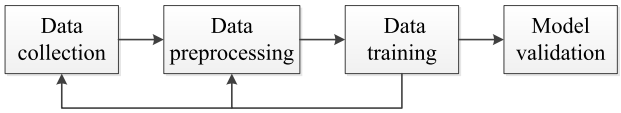

FIGURE 5. Process of supervised learning to solve classification problems.

Typical algorithm of semi-supervised algorithm include deep learning [43] and k-means.

In the problem of underground target classification in this paper, we use the simulation data generated by the spheroid model. The general process of supervising learning to solve classification problems is shown in the figure 5 [41]. Taking the example of target material classification, the first step is data collection. The simulation data of various sizes and materials are generated by spheroid model or the approximate forward model, and the material is used as the sample label. The second step is data preprocessing. The quality of data collected in the actual scene is uneven. We need to filter the data to find high-quality data. In this paper, we use the simulated data generated by the model as the classified data set. The data quality is controllable, which eliminates the operation of this step. In the third step, data training, we divide the available data into training set and test set with non-coincident data, and select different classifiers to learn the training sets. The final step is model validation, and the model completed by the training is utilized to predict the test set label, and the performance of the classification algorithm is evaluated by comparing with the real label of the test set.

At the beginning of the study, we used 12 commonly used classification algorithms to classify object material and shape. We selected the eight classifiers with the highest classification accuracy as the classification algorithm studied in this paper. In order to find the best classifier in the underground target detection, we further evaluated the eight algorithms with classification accuracy, recall, precision and confusion matrix. In the future work, the parameters of the best classifier are further optimized to achieve a more accurate classification result.

A. CLASSIFICATION ALGORITHM

There are numerous types of supervised classification algorithms, which can be roughly divided into generative classifiers and discriminative classifiers [44]. The central idea of generative classifier is to obtain the joint probability $P(x, y)$ though the data, and then calculate the conditional probability distribution $P(Y|X)$ by Bays rules as the prediction model. The typical generation model is Quadratic discriminant analysis (QDA). The central idea of discriminant classification is to directly learn the decision function through data as the prediction model, such as decision tree (DT), support vector machines (SVM), Gaussian process (GP), neural networks (NN) and ensemble learning. SVM is a classification algorithm based on the kernel method. In this paper, the support vector machine with the linear kernel (SVM-LK) and the polynomial kernel (SVM-PK) are realized. Ensemble

learning is a series of classification algorithms that integrate the prediction results of multiple classifiers. In this paper, the random forest (RF) algorithm and the adaboost algorithm are implemented.

Taking the classification of the target shape with known orientation as an example, and given a data set $D = \{(x_1, y_1), (x_2, y_2), \cdots, (x_m, y_m)\}$, the sample $x_i = \{k_1, \alpha_1, \beta_1, k_2, \alpha_2, \beta_2,\}$ is a vector described by six attributes. k_1, α_1, β_1 are the parameter of polarization tensor $L_2(t)$ parallel to the major axis of the axi-symmetric target. k_2, α_2, β_2 are the parameter of polarization tensor $L_1(t)$ perpendicular to the major axis of the axi-symmetric target. $C = \{y_1, y_2, \cdots, y_n\}$ indicates the collection of the sample labels, and y_i indicates the class of target shape to which the ith sample belongs, we divided the target shape into two labels $y_i = \{-1, +1\}$.

1) QUADRATIC DISCRIMINANT ANALYSIS

One of discriminant analysis is linear discriminant analysis (LDA), which calculates the posterior probability function of each class on the basis of Bayes' theorem, and monotone function is superimposed on the function to generate a linear decision surface.

The algorithm flow of LDA is introduced in [45]. In this paper, we utilized the QDA algorithm to classify the simulation data. The distinction between LDA and QDA is the different covariance matrix. The former assumes that the covariance matrices of each class are the same, and the latter assumes that the covariance matrices of the classes are different from each other. The decision function of QDA is expressed as:

$$\delta_k = -\frac{1}{2}(x-\mu_k)^T \sum^{-1} (x-\mu_k) - \frac{1}{2}\log\left|\sum_k\right| + \log \pi_k \qquad (18)$$

where μ_k is the mean value of sample in different classes, and $\sum_k$ is the covariance matrix.

2) GAUSSIAN PROCESS

The Gaussian process (GP) is a stochastic process, in which the joint probability density of a series of continuous domain random variables is a gaussian distribution. The flow and details of the algorithm are introduced in [46]. The kernel of the Gaussian process is a crucial part of determining the shape of priori and posterior of the Gaussian process, mainly used to compute the covariance between datapoints. In this paper, we use the radial-basis function (RBF) kernel as the covariance function of the Gaussian process, which can be defined as:

$$k(x_i, x_j) = \exp\left(-\frac{1}{2}d(x_i/l, x_j/l)^2\right) \qquad (19)$$

l is a length-scale parameter with a value greater than 0, which is utilize it to parameterize the covariance function. In this paper, l is taken as 1.

TABLE 1. kernel functions.

Name	Expression	Decision function
linear kernel	$K(x_i, y_j) = (x_i \cdot y_j)$	$f(x) = \operatorname{sgn}\left(\sum_{i=1}^{t} a_i y_i (x_i \cdot y_j) + b\right)$
polynomial kernel	$K(x_i, y_i) = (\gamma \langle x_i, x_j\rangle + r)^d$	$f(x) = \operatorname{sgn}\left(\sum_{i=1}^{t} a_i y_i (\gamma \langle x_i, x_j\rangle + r)^d + b\right)$

3) SUPPORT VECTOR MACHINES

Support Vector Machine algorithm is developed from choosing the best hyperplane in linear classification. In this paper the training data in sample space is nonlinear separable [22], [27].

We map the original sample space into the feature space where training data are separated by the kernel function. Next, we fit the best hyperplane. After mapping for original sample space by kernel function, the decision function is as follows:

$$f(x) = sgn\left(\sum_{i=1}^{m} c_i y_i K(x_i, y_j) + d\right) \qquad (20)$$

where c_i and d are the parameters of the best hyperplane, $K(x_i, y_j)$ is the inner product after $\langle x_i, y_i\rangle$ is mapped, and function K is the inner product kernel function for feature mapping.

The kernel functions and the corresponding decision functions used in this paper are shown in the following table:

The linear kernel is the simplest kernel function. It is given by the inner product $\langle x_i, y_i\rangle$ plus an optional constant C. The polynomial kernel represents the similarity of vectors (training samples) in a feature space over polynomials of the original variables. γ is the scaling parameter. d is the degree of the polynomial. In this paper, $C = 1$, $\gamma = 1/6$, d is taken as 3.

4) DECISION TREE

The decision tree model is a tree-like model that classifies samples based on features. The chief steps of classification are tree construction and tree pruning.

In the tree construction, attribute selection is the critical step, which can help us select the attributes used in the classify problem to achieve a good result. The CART algorithm is implemented in this paper, which constructs decision trees by Gini index.

The Gini index is a attribute selection metric used to describe the purity of the data set. The definition of Gini index is shown in [47], [48]. The construction of decision tree is to repeatedly find the node with the smallest Gini index and split the training data set until the termination condition is met.

The purpose of tree pruning is to avoid over-fitting problems. Tree pruning is divided into pre-pruning and post-pruning. The pre-pruning method used in this paper is to set the maximum depth of the sub-tree. we set $\max\_depth = 5$. The post-pruning method generates a sub-tree sequence by calculating the loss function of the sub-trees, and then the optimal sub-trees are selected as the final decision tree through cross-validation.

5) RANDOM FOREST

Random forest (RF) belongs to ensemble learning. It utilizes the decision tree as the base estimator, and it combines the prediction results of each base estimator to improve the performance of random forest. The sample of the construction decision tree is obtained from a sample drawn with replacement from the training set. In attribute selection, we chose the best attribute among the random subset of attributes for split training set. The prediction result of the random forest is obtained by averaging the prediction probabilities of each estimator [49].

When the random forests is used in classification, there are three parameters that need to be adjusted: N_e, $\max_f$, and $\max_d$. N_e represents the number of decision trees in the forest. In this paper, $N_e = 10$; $\max_f$ is the size of the random subset of attributes when the node is split. In this paper, $\max_f = 3$; $\max_d$ is the maximum depth when the decision tree is generated, and we set $\max_d = 5$.

6) ADABOOST

Adaboost is an iteration algorithm. The main idea of Adaboost is to train various weak learners for the same training set and boost these weak learners to a strong one. In the process of iteratively boosting in the weak learner, the weights of data which were incorrectly predicted by the weak learner at the previous boosting iteration are increased, and the weights are decreased for those that were predicted correctly. Finally, the combination of the weak learners is used as a strong one. The weak learners with the small classification error rate are given a large weight, and the weak learners with the large classification error rate are given a small weight [50]. The implementation details are as follows:

a): Assume that the weights of training data set are uniformly distributed. The basic classifier $G_1(x)$ is learned from the training data.

b): AdaBoost is learned the basic classifier repeatedly, and performed the following operations in sequence in each learning round, where m represents the learning round:

Learn the basic classifier $G_m(x)$. Using the data set D_m with the current weighted distribution.

Calculate the classification error rate e_m of the basic classifier $G_m(x)$ on the training data set D_m.

Calculate the coefficient α_m of the basic classifier $G_m(x)$. α_m indicates the importance of $G_m(x)$ in the final classifier. The smaller the classification error rate, the greater the role of the basic classifier in the final classifier.

Update the weight distribution of the training data to prepare for the next round.

Increase the weight of the misclassified samples by the basic classifier $G_m(x)$, and reduce the weight of the correctly classified sample. So that the misclassified sample plays a greater role in the next round of learning.

c): We constructed the combination $f(x)$ of the weak learners to implement weighted majority voting of the M weak learners.

$$f(x) = \sum_{m=1}^{M} \alpha_m G_m(x) \tag{21}$$

The parameter α_m represents the importance of the weak learners, and the number of weak learners $M = 50$.

7) NEURAL NETWORKS

The neural network (NN) is a mathematical model or computational model that mimics the structure and function of the biological neural network [51]. The algorithm details of NN are introduced in [52].

For the nonlinearly separable problems, it can be solved by utilizing the multi-layer functional neurons. The multi-layer perceptron(MLP) with one hidden layer was used in this paper.

The input layer represents the input attributes, and it can transmit the signal from the artificial neuron in input layer to another artificial neuron in the hidden layer. The rectified linear unit function is used as the activation function in this paper, its form is $f(x) = \max(0, x)$.

The process from the hidden layer to the output layer can be seen as a softmax regression. The stochastic optimizer have been used to determine the weight of different layers, which improves the prediction accuracy [53].

B. PERFORMANCE METRICS OF CLASSIFICATION ALGORITHM

After introducing various classification algorithms, it is essential to measure the performance of different algorithms. The measurement criterion is called performance metric. Generally, performance metrics reflect the task requirements, and different evaluation results will be presented in the same algorithm when judged by different performance metrics. There are five performance metrics are discussed in this section: accuracy, error, confusion matrix, precision and recall.

1) ACCURACY AND ERROR

Generally, the metric for evaluating classifier performance of the classifiers is the accuracy, which is defined as the proportion of the samples correctly classified by the classifier in the test data set. The opposite concept is the error, which is the proportion of the samples incorrectly classified by the classifier in the test data set. For sample set D, they are defined as:

$$\begin{aligned} Accuracy &= \frac{TP + TN}{TP + TN + FP + FN} \\ Error &= \frac{FP + FN}{TP + TN + FP + FN} = 1 - Accuracy \end{aligned} \tag{22}$$

Taking the binary classification problem as an example, we can divide the sample into true positive, false positive, true negative, false negative according to the true class and the prediction class. TP, FP, TN, and FN indicate the number of samples in the corresponding class, respectively.

TABLE 2. confusion matrix of the binary classification problem.

True class	Predicted class	
	Positive	Negative
Positive	TP	FN
Negative	FP	TN

2) OTHER PERFORMANCE METRICS

Accuracy and error are common performance metrics, but they are unable to satisfied various task requirements. Taking the classification problem in this paper as an instance, if we are concerned about the ''the proportion of the misclassified samples in the samples classified as non-metallic class'' or ''the proportion of the correctly classified sample in the sample which true class is metal'', the error and accuracy are unable to intuitively describe the problem. Therefore it is essential to utilize additional performance metrics.

The confusion matrix is a visualization tool frequently used in supervised learning, which can represent the classification performance of the classification model on every class [54]. The confusion matrix of the binary classification problem is shown in table 2:

The precision P represents the proportion of the correctly classified samples in the samples predicted as positive class, which is defined as [55]:

$$P = \frac{TP}{TP + FP} \tag{23}$$

The recall R represents the proportion of the correctly classified samples in the samples of which real class is positive, which is defined as [55]:

$$R = \frac{TP}{TP + FN} \tag{24}$$

VI. SIMULATION VERIFICATION

In order to verify the classification feasibility and analyze the factors that may affect the classification results in the classification process. Firstly, we implemented the spheroid model and approximate forward model, and generate the simulation data. Secondly, we have analyze the simulation data. Lastly, the classification algorithm is implemented, and the classification performance is analyzed.

A. SENSITIVITY ANALYSIS RESULTS

In this part, sensitivity analysis has been performed on the spheroid model and the approximate forward model.

1) SPHEROID MODEL

In the spheroid model, the parameters are related to the magnetic permeability which describe the target material, and the radius which describe the shape of the target. However, the influence of the target properties (material and shape) on the parameters is currently undetermined. It is difficult to evaluate the distinguishing ability of different model parameters on the classification of target properties. Therefore, it is essential to utilize different tools to analyze and verify the influence. We analyze the relationship between each parameter and the target properties from two aspects: sensitivity analysis and distribution of simulation data. Taking the sensitivity analysis of the parameter model α as an example, expression of α is:

$$\alpha = \frac{a \cdot \sigma \mu_r \mu_0 R^2}{(\mu_r + 2)(\mu_r - 1)} \tag{25}$$

In the formula, σ is the conductivity. μ_0 is the vacuum permeability. We take them as the fixed value ($\sigma = 37667620.91$, $\mu_0 = 1.2566370614 * 10^{-6}$). μ_r is the relative permeability and R is the radius of the sphere, we take them as the variables in (25).

In the spheroid model, μ_r and R are independent variables. Assuming that variables are uniformly distributed over the specified range:

$$\begin{aligned} 2 \le \mu_r \le 100 \\ 0m \le R \le 2m \end{aligned} \tag{26}$$

The mathematical expectation(E) and variance(V) of the variables are:

$$\begin{aligned} E_{\mu_r} &= 49, \quad E_R = 1 \\ V_{\mu_r} &= 800.333, \quad V_R = 0.333 \end{aligned} \tag{27}$$

where E_{μ_r} and E_R are the mathematical expectation of relative permeability μ_r and the sphere's radius R, respectively. V_{μ_r} is the variance of μ_r, and V_R is the variance of R.

Plugging the value obtained in (27) and (9) into equations (14) (15) (16) and (17), the output uncertainty of the model and the contribution of each variable to output uncertainty can be obtained:

$$\begin{aligned} V_\alpha &= 3.201, \quad S_{\mu_r} = 0.147 \\ S_R &= 0.658, \quad S_{\mu_r R} = 0.195 \end{aligned} \tag{28}$$

where V_α is the output uncertainty of the parameter α model. S_{μ_r} and S_R are the importance of μ_r and R in determining the output uncertainty, respectively. $S_{\mu_r R}$ is the importance of the interactions between the μ_r and R in determining the output uncertainty.

Since S_R is the biggest, variable R contributes greatly to the uncertainty of model output. S_R and $S_{\mu_r R}$ are relatively small, although the variable μ_r and the interactions between the variables have an effect on determining the output uncertainty, their influence is smaller than the that of radius. For other parametric models, the procedures for performing sensitivity analysis are similar to the previous example. Assuming that the distribution range of the input variables remains unchanged, the measures of sensitivity in other parameter models(K, α, β) are shown in the following table:

For the parameter K and β, since S_R is larger and S_R and $S_{\mu_r R}$ are smaller, the variable R plays a decisive role in determining the output uncertainty, besides, the contribution of the interactions between the variables and the variable μ_r to the output uncertainty are negligible.

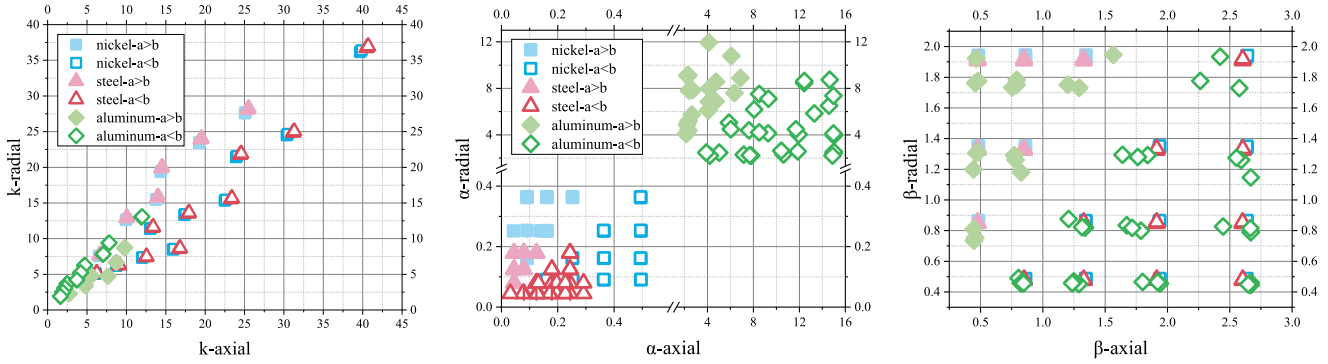

(a) parameter K (b) parameter α (c) parameter β

FIGURE 6. The distribution of different parameters for various size and material spheres. Plot (a) illustrates the distribution of parameter K. Plot (b) illustrates the distribution of parameter α. Plot (c) illustrates the distribution of parameter β. (a) parameter K. (b) parameter α. (c) parameter β.

TABLE 3. The measures of sensitivity in other parameter models.

Sensitivity	Parameter K	Parameter α	Parameter β
S_{μ_r}	$1.763 * 10^{-6}$	0.147	$2.241 * 10^{-6}$
S_R	0.999	0.658	0.999
$S_{\mu_r R}$	$5.291 * 10^{-6}$	0.195	$2.298 * 10^{-6}$

For all parameter, the influence of variable R on determining the output uncertainty is generally greater than that of μ_r. R is a variable directly related to the target shape, μ_r is a variable which can represent the class of target material to a large extent. Thus in the classification of objects, it is speculated that the classification performance of shape-based labeling is better than the material-based labeling according to the sensitive analysis.

Next, we verify the results by visually analyzing the simulation data. By utilizing the spheroid model to generate the simulation data of various materials and shapes, and mapping the distribution of the data at different parameters, a more intuitive relationship between the parameters and the properties of the target can be exhibited.

The simulation data is generated by the spheroid model, in which the equatorial radius a and the polar radius b are in the range of 0.6-1.4 and the step is 0.2. The target materials are divided into three classes: nickel, aluminum and steel. Steel and nickel are permeable materials, and the aluminum is non-permeable material. We collect the simulation data on the transverse axis and the axial axis, and the distribution of simulation data with different parameters is shown in Fig. 6.

As can be seen from Fig. 6(a), the data points of the permeable spheroids and the non-permeable spheroids are concentrated in different regions. After determining the material, the spheroids with different sizes can also be separated according to the data points. However, when the K is in the range of 0-15, the data points of the spheroids with different materials and shapes overlap each other. Thus, the simulation data distribution of the parameter K can distinguish the material permeability in a specific range, but the distinguishing ability among the permeable materials is weak. In the distinction of target shape, after the target material is determined, the shape can be roughly distinguished, but the distance of data points in distribution map is relatively close.

It can be seen from Fig. 6(b) that the distribution region of the data points of permeable spheroids and the non-permeable spheroids are far apart, and the data points of permeable spheroids overlap where α is in the range between 0 and 0.3. The data points of spheres with different shapes are clearly separated. Thus, the distribution of the parameter α can relatively clearly distinguish the target material, even for the permeable materials, the distinguishing ability is stronger than that of parameter K. The shape can be distinguished without prior knowledge of the material.

As can be seen from Fig. 6(c), the data points of spheroids with different materials are basically overlapping, and the data points of spheres with different shapes are clearly separated. Thus, it is found that the material cannot be distinguished by the single parameter β, but the shape can be distinguished clearly.

Based on the distribution of the Fig. 6 and the previous description, it can be concluded that we are unable to classify materials accurately with three parameters. Even for the parameter α – which has preferable performance compared with other parameters in the material classification, the data distribution is still overlapped in distinguishing the permeable material, which is more likely to be misclassified in the classification. In the distinguishing of the shape, the stimulation data have a clear separation in the distribution of the parameters α and β. Thus, from the perspective of data distribution, the classification performance on the shape is superior than the case on the material in the same data set.

2) THE APPROXIMATE FORWARD MODEL

The properties of the target can be classified according to the model parameters of the spheroid model. However, in a real measurement scene, the target orientation is uncertain. In order to simulate the real measurement scene, the approximate forward model has been introduced in section 2. The main idea is to join the influence of orientation parameters

on the basis of the spheroid model. Thus, if we want to classify objects utilizing parameters in the approximate forward model, consideration about the effect of the orientation on the model output uncertainty is essential. We quantify the effect by sensitivity analysis. If the influence of the orientation on the output is greater than the target's property parameters (e.g. equatorial radius, polar radius of spheroid), it can be inferred that classifying objects with unknown orientation is not feasible. Similarly, if the contribution of the orientation to the output is negligible, it is meaningful to classify objects with unknown orientation. Therefore, we analyze the approximate forward model with the sensitivity analysis and parameter distribution.

In the sensitivity analysis of the spheroid model, the contribution of the relative permeability to the parameters(K, α, β) is relatively small, and the radius plays a decisive role in determining the parameters output uncertainty. Thus, in the approximate forward model, we analyze the contribution of orientation and radius to the parameters function.

The property variables of the target model that we are interested in are the polar radius a and the equatorial radius b. In the orientation variables, since the axi-symmetric target was the main research target in the approximate forward model, the change of the heading angle(ψ) does not affect the coordinate transformation. So we mainly focus on the pitching angle(θ) and the roll angle(ϕ). The simplified approximate forward model is shown as:

$$\begin{aligned} M &= U(\theta,\phi)\cdot\overline{\overline{M}}(\mu_r,a,b,t)\cdot U(\theta,\phi)^T \\ \overline{\overline{M}} &= \begin{pmatrix} L_2(\mu_r,a,b,t) & 0 & 0 \\ 0 & L_2(\mu_r,a,b,t) & 0 \\ 0 & 0 & L_1(\mu_r,a,b,t) \end{pmatrix} \end{aligned} \tag{29}$$

where U and U^T are transformation matrixes; L_n is the polarization tensor in different directions of the spheroid model. Due to the fact that it is not required to analyze the contribution of relative permeability to the model, and the major target we detected is permeable object, we set $\mu_r = 1000$. The contribution of time parameter to the model is not our research objective, so $t = 0.08s$ [22].

In this paper, we focus on the classification of prolate spheroid whose polar radius b is greater than equatorial radius a. The radius (a, b) and the orientation(θ, ϕ) are independent variables. Assuming the variables are uniformly distributed over the specified range:

$$\begin{aligned} 0m \le a \le 0.2m, &\quad 0.8m \le b \le 1m \\ 0^\circ \le \theta \le 120^\circ, &\quad 0^\circ \le \phi \le 120^\circ \end{aligned} \tag{30}$$

The mathematical expectation(E) and variance(V) of the variables are:

$$\begin{aligned} &E_a = 0.1, E_b = 0.9, \quad E_\theta = 60, E_\phi = 60, \\ &V_a = 0.0033, \quad V_b = 0.0033, \; V_\theta = 1200, \; V_\phi = 1200 \end{aligned} \tag{31}$$

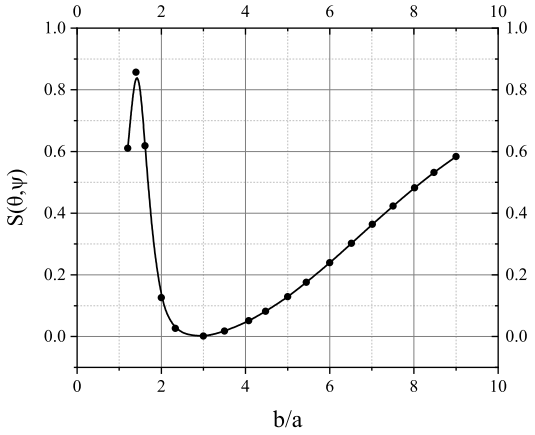

FIGURE 7. The contribution of the orientation variable to the model output uncertainty with varying aspect ratios.

where E_a, E_b, E_θ and E_ϕ are the mathematical expectation of equatorial radius a, polar radius b, pitching angle θ and roll angle ϕ, respectively. $V(a)$, $V(b)$, $V(\theta)$ and $V(\phi)$ are the variance of a, b, θ and ϕ.

The procedure of sensitivity analysis is the same as that of spheroid model, the output uncertainty of the model and the contribution of each variable to the output uncertainty can be obtained. Since the calculation of the influence of interactions between the variables on model output is complicated, and the influence of the single orientation variables (θ, ϕ) can clearly show the influence of the orientation variables on the model output, we do not consider the contribution of interactions between the variables to model output:

$$\begin{aligned} &V_\alpha = 0.1782, \quad S_a = 0.4141, \quad S_b = 0.0022, \\ &S_\theta = 0.068\,, \quad S_\phi = 0.577 \end{aligned} \tag{32}$$

where V_α is the output uncertainty of the parameter α of the approximate forward model. S_a, S_b, S_θ and S_ϕ are the importance of radius variable a, radius variable b, orientation variable θ and orientation variable ϕ in determining the output uncertainty.

The orientation variable θ and ϕ have has a greater contribution on the model output uncertainty, so the results of classify targets with unknown orientation is inaccurate. In order to verify the influence of orientation variables, we performed sensitivity analysis on various size spheroids. The result is shown in Fig. 7.

Fig. 7 exhibits the influence of orientation variables on model output when the aspect ratio of the permeable target is different. The ratio is b/a, $S(\theta, \phi)$ is the sum of the first-order indices of the roll angle and the pitching angle. θ and ϕ are in the range between 0° and 120°. The figure shows that the first-order indices of the orientation variable has obvious fluctuation when the aspect ratio between 1 to 2. When the aspect ratio is 1.4, $S(\theta, \phi)$ reaches the peak. Since then, it shows a significance downward trend. For spheroid with the $b/a = 3$, $S(\theta, \phi)$ reaches the minimum. When the aspect ratio is greater than 3, $S(\theta, \phi)$ shows a slow raise trend.

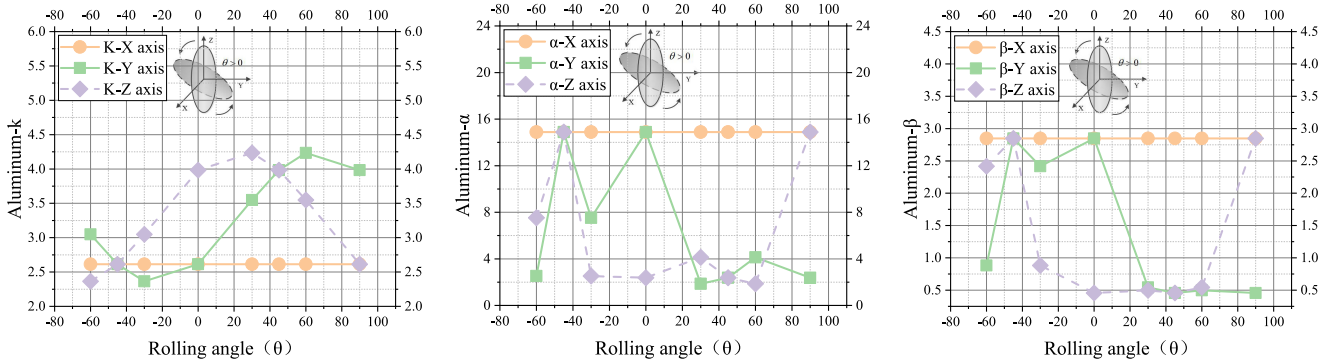

(a) parameter α (b) parameter K (c) parameter β

FIGURE 8. The parameter (K, α, β) of aluminum target with varying orientations (θ). (a) parameter α.

As shown in Fig. 7, the influence of the orientation in determining the model output is usually large, so objects are unable to be effectively classified when the orientation is unknown. The orientation can be obtained by filter estimation [56] and inversion method [57], [58]. In this paper, we will focus on the objects classification with known orientation. Next, we analyzed the simulation data visually to verify that objects classification is not feasible when orientation is unknown.

The simulation data is generated by the approximate forward model. The polar radius $b = 1.5m$, equatorial radius $a = 0.6m$, the material is aluminum, the rolling angle is in the range from $-90°$ to $90°$ and the step is $30°$. Parameter in the approximate forward model are treated as functions of rolling angle and the orthogonal axes, and the results are provided in Fig. 8.

Figure 8 suggests that the K, α and β in the approximate forward model may not be used to classify the target. In each subgraph, the variation of the parameters is irregular, which confirm that it is not feasible to classify objects with unknown orientation.

B. INFLUENCE OF ORIENTATION ON CLASSIFICATION RESULTS

In the previous section, we analyzed the effect of the orientation on the approximate forward model output. Ultimately, we find that objects classification with unknown orientation is not feasible. In this section, we utilize the approximate forward model to generate simulation data sets. The simulation data sets are used as the training and test data of the machine learning algorithms for objects classification, and the classification results of the eight algorithms are compared to further verify that objects classification with unknown orientation is not feasible. The comparison of classification results is shown in Fig. 9.

We generated the parameters of spheroids with various size and material as simulation data sets. The orientation is a random parameter. The equatorial radius a, polar radius b are between 0.5m and 1m, and the target material is divided into three classes: nickel, steel and aluminum. The target shape

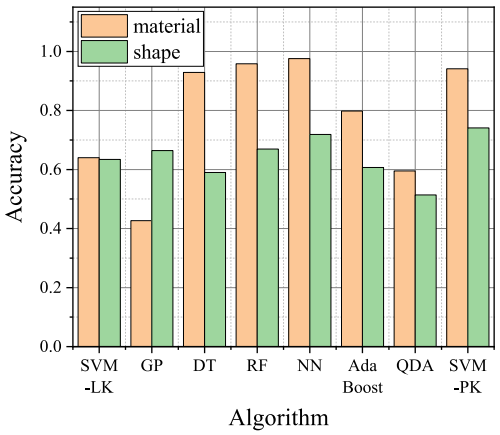

FIGURE 9. The behavior of classification accuracy for various size and material spheroids with different machine learning algorithms.

is divided into two classes according to aspect ratio: aspect ratio$>$1, aspect ratio$<$1.

When classifying the target shapes, the classification accuracy of each classifier is generally low, basically less than 70%. Compared with other algorithms, the SVM with polynomial kernel achieves the best accuracy of 0.741, which fully testifies that the orientation influences the classification performance seriously. When classifying the target materials, half of the classifiers have low classification accuracy. The accuracy score of the Gaussian process is the lowest, even worse than random guess. However, the accuracy of some classifiers reaches 90%, which is inconsistent with the previous conclusions. For this situation, we initially presume that there was an error in fitting the simulation data. In order to accurately estimate the model parameters, it is essential to obtain the upper and lower bounds of the target parameters. However, it is unable to obtain the exact bounds in current research, so we set the bounds more broadly. This lead to the simulation data fitted by fitting algorithm may not precise – the simulation parameters infinitely approach the upper or lower bounds, thus the classification accuracy is not consistent with the expected situation.

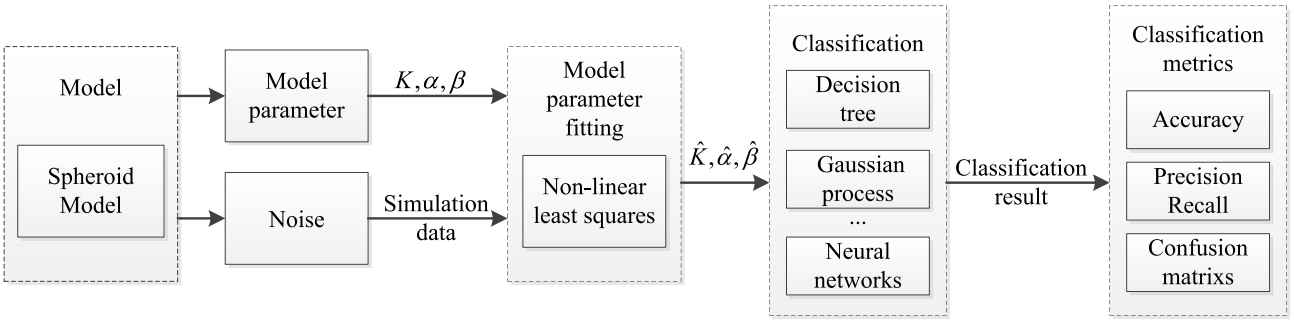

FIGURE 10. The classification process of the model-based method.

C. CLASSIFICATION RESULTS COMPARISON

The factors affecting the classification attributes (model parameters) are analyzed and summarized previously, but there are various other factors that affect the classification performance in the classification process.

The classification process is shown in Fig. 10. First, simulation data and true model parameters (K, α, β) are generated by the spheroid model. Secondly, we add noise at different SNR to the simulation data and obtain the fitted model parameters $(\hat{K}, \hat{\alpha}, \hat{\beta})$ by the fitting algorithm (Non-linear least squares). Next, we use the fitted model parameters as the classification attributes and classify the material and shape of the target by eight algorithms. Finally, the classification results are evaluated by accuracy, recall, precision and confusion matrix.

Afterward, we analyze the impact on the classification results from the perspective of the fitting algorithm and classification algorithm.

1) INFLUENCE OF FITTING ALGORITHM ON CLASSIFICATION PERFORMANCE

In the real measurement scene, the secondary magnetic field response detected by the receiver is usually interfered by the geomagnetic field, which requires the anti-noise ability of the classification algorithm. Thus, we add noise at different SNR to the simulation data and obtain the model parameters by fitting algorithm at first, and we compare the errors between the true model parameters (K, α, β) and the fitted model parameters $(\hat{K}, \hat{\alpha}, \hat{\beta})$ to obtain the influence of noise on the fitted parameters $(\hat{K}, \hat{\alpha}, \hat{\beta})$. Afterwards, the model parameters obtained from noise-added data sets as the classification attributes, and the shape and material are utilized as classification labels. We analyze the influence of the fitting algorithm on the classification performance by comparing the performances of eight classification algorithms. Next, the influence of noise on the fitted parameters and the influence of the fitting algorithm are analyzed from the perspective of classification label: material-based classification and shape-based classification.

Specifically, in material-based classification and shape-based classification, the simulation data are generated by the spheroid model, the added noise is in the range between 0dB and 40dB. The fitting algorithm is non-linear least squares. After the simulation data is fitted, the fitted model parameters are obtained. The errors between the true model parameters (K, α, β) and the fitted model parameters $(\hat{K}, \hat{\alpha}, \hat{\beta})$ in material-based classification are shown in table 4. The errors between the true model parameters (K, α, β) and the fitted model parameters $(\hat{K}, \hat{\alpha}, \hat{\beta})$ in shape-based classification are shown in table 5.

TABLE 4. The errors of material-based classification.

SNR of added noise	Error of nickel	Error of steel	Error of aluminum	Average error
10 dB	120.61%	100.41%	142.75%	121.26%
20 dB	60.93%	42.54%	110.81%	71.42%
30 dB	24.42%	14.67%	89.41%	42.83%
40 dB	9.22%	5.44%	79.83%	31.49%

TABLE 5. The errors of shape-based classification.

SNR of added noise	Error of $a > b$	Error of $a < b$	Average error
10 dB	129.58%	114.82%	121.26%
20 dB	74.69%	68.90%	71.42%
30 dB	43.52%	42.30%	42.83%
40 dB	32.69%	30.57%	31.49%

The target label is divided into three classes in material-based classification: nickel, steel and aluminum. It can be seen from the table 4 that the average error and the error of three materials (nickel, steel and aluminum) decrease with the SNR increases. It indicates that the added noise has a greater impact on the accuracy of the fitted model parameters. In other words, the smaller the SNR is the worse the performance of the fitting algorithm. However, when the SNR is 30dB or 40dB, the error of nickel and steel is less than 30%, but the error of aluminum is more than 79%. It indicates that when the SNR is large, the non-linear least squares algorithm can accurately fit the model parameters of permeable materials (nickel and steel), but it is unable to accurately fit the model parameters of non-permeable materials (aluminum).

As shown in Table 5, the target label is divided into two classes in shape-based classification: a>b, a<b. The former represents an oblate spheroid and the latter represents a prolate spheroid. a is equatorial radius, b is polar radius. As same

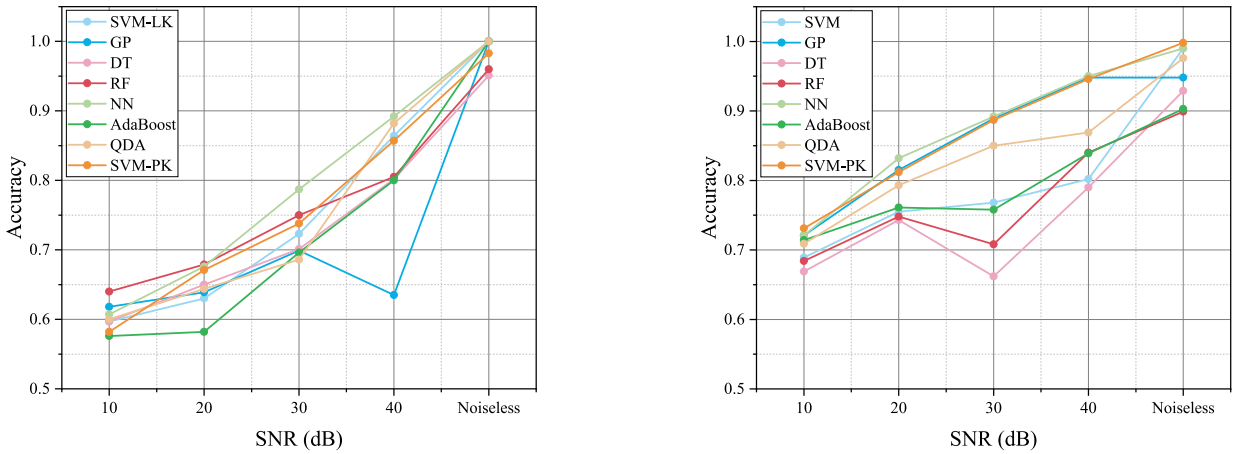

(a) material-based labeling

(b) shape-based labeling

FIGURE 11. Relating the SNR of added-noise with the classification metric (accuracy).

as table 4, that the average error and the error of two shapes (a>b and a<b) decrease with the SNR increase. It indicates that the added noise has a greater impact on the accuracy of the fitted model parameters. When the SNR is 10dB, the error of two shapes(a>b and a<b) is approximately 120%. When the SNR is 40dB, the error of two shapes is about 30%.

After the simulation data and model are fitted, the classification performances of various classification algorithms is measured by accuracy. The influence of the fitting algorithm is analyzed from the perspective of classification label: material-based classification and shape-based classification.The accuracy of eight classifiers in material-based classification is shown in Fig.11(a). The accuracy of eight classifiers in shape-based classification is shown in Fig.11(b).

Fig.11 exhibits that all classifiers achieve a high classification accuracy when noise-less simulation data is used as the classification data. However, as the SNR decrease, the classification accuracy of the classifier is getting worse. It reflects that the anti-noise ability of the classification algorithm still demands to be strengthened. Combining the results of Fig.11, table 4 and table 5, we found that the performance of the fitting algorithm is relatively poor, the parameter is fitted more accurate only when the SNR is high. Thus, in order to improve the classification accuracy, it is essential to improve the fitting results of the fitting algorithm at low SNR in future research.

By comparing Fig. 11(a) and Fig. 11(b), it is obvious that when the data set at the same SNR, the classification performance of shape-based classification is better than the material-based classification. In the meantime, this also confirms the results that we have obtained in the sensitivity analysis of the spheroid model. Overall, the classification accuracy are sensitive to the noise level, which provides a follow-up research perspective for improving classification accuracy.

2) INFLUENCE OF DIFFERENT CLASSIFIERS ON CLASSIFICATION PERFORMANCE

In this section, the performance of the proposed method was evaluated in term of accuracy, recall, precision and confusion matrix which are related to the sample distribution. In addition, the obtained results were evaluated and compared with different machine learning such as SVM, NN, and DT, etc.

To further improve the accuracy of underground metal classification, we want to select the classifier that is most suitable for underground metal classification problems by comparing the performance of different classifiers, and further enhance its classification ability in future work.

Generally, in the performance evaluation of the precision and recall, the classification algorithm is considered to be effective only when the values of both are high and the gap between them is small. However, the recall and the precision are a pair of contradictory metrics, which implies that it is difficult to achieve the above evaluation criteria. Therefore, in different fields of application, we will pay close attention to one of the metrics according to actual demands. In the detection of underground targets, the recall is the more critical metric. Especially in the material-based classification, if metal targets (unexploded ordnance and landmine) are not predicted in the classification, they may not only damage human's life but also be destructive to property, environment and resources,etc.

We still utilize the target material and shape as the classification label. In order to simulate the reality, we choose the data set with SNR is 30dB as the data set to be fitted, and the fitted data are utilized as the training data for the classification algorithm. Afterward, the classification performances of different classification labels are analyzed based on the same classification metrics. Above all, we evaluated the classification performances of the classifiers by accuracy, recall and precision. We used the hold-out method to

TABLE 6. precision and recall of material-based classification.

Algorithm	Aluminum		Nickel		Steel	
	precision	recall	precision	recall	precision	recall
SVM-LK	97.4%	74.7%	73.1%	49.2%	59.5%	92.9%
GP	91.4%	85.9%	60%	54.3%	60.3%	69.7%
DT	99.4%	77.3%	69.1%	42.7%	56.3%	90.4%
RF	96.7%	89.9%	73.3%	48.2%	61.4%	86.9%
NN	94.9%	85.4%	71.1%	66.8%	72.2%	83.8%
AdaBoost	96.1%	86.4%	56.6%	45.2%	59.3%	77.3%
QDA	100%	67.2%	73.9%	42.7%	54.8%	96%
SVM-PK	90.5%	86.9%	67.1%	54.3%	65.2%	80.3%

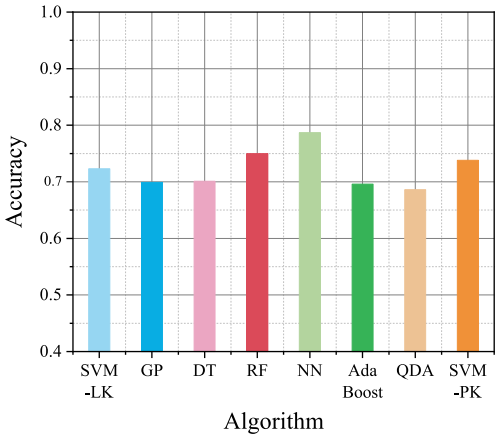

FIGURE 12. The results of material-based classification by accuracy.

evaluating the classifiers performance. The hold-out method divides the dataset into two mutually exclusive sets, one as a training set and the other as a test set. 2973 data are included in the dataset. We use 4/5 of the dataset as a training data, the remaining 1/5 as a test data. The results of material-based classification are shown in Table 6 and Fig. 12:

Table 6 indicates the precision of aluminum is higher than the recall and the gap between the two is small. The recall of steel is higher than the precision, but the gap is bigger than the gap between the precision and recall of aluminum. The precision of nickel is higher than the recall, but the performance of the both is poor. This implies the classification performance of nickel is worse than the other two materials. Fig.12 exhibits that the accuracy of the classifiers is concentrated between 68%-80%, the accuracy of neural network classifier is the highest among the eight classifiers.

In the classification results of aluminum, the QDA algorithm exhibited the highest precision but the lowest recall. It is indicated that although a large percentage of the samples predicted by the classifier are correct, only 68% of the aluminum-label samples in the real data set are identified, the remaining aluminum-label samples were misjudged as other materials. Other algorithms have also displayed the similar problems. Thus, it is essential to further improve the recall in the future research. It is worth mentioning that neural networks and adaboost have a higher precision while ensuring smaller gaps between the precision and the recall than other classifiers. Therefore, in the classification of aluminum

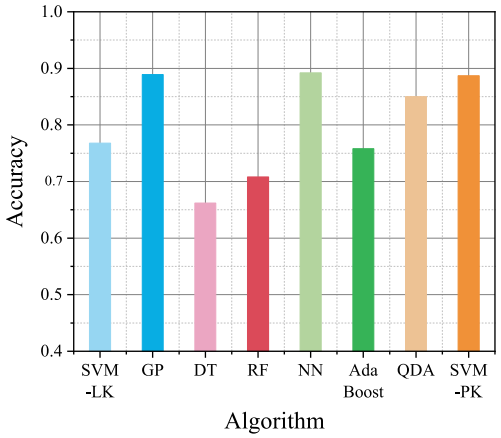

FIGURE 13. The results of shape-based classification by accuracy.

materials, the classification performance of neural network and adaboost is better than other algorithms.

In the classification results of steel, the SVM with linear kernel algorithm exhibited a higher recall but lower precision. It is indicated that 93% of the steel-label samples in the real data set are predicted correctly, but only 60% of the sample labels predicted to be steel are correct. Although other algorithms have similar flaws, the neural network have a high recall while ensuring a relatively small gap between the precision and recall. Therefore, in the classification of steel, the classification performance of neural network is better than other algorithms. Although we are more emphasize the recall than the precision, the low precision will result in excessive consumption of manpower and resources(mining underground targets). Therefore, it is necessary to increase the precision moderately while ensuring that the recall is not reduced.

In the classification results of nickel, the adaboost algorithm exhibited a higher precision but lower recall, other algorithms also present a trend like this. However, the recall and precision are low compared with other materials, thus the classification performance is poor. It is worth mentioning that in the neural network, the gap between the recall and the precision is the smallest. Therefore, in the classification of nickel, the classification performance of neural network is better than other algorithms.

In the accuracy assessment of various classifiers, the neural network displays the highest accuracy. From the Table 6, we can observe that the recall and precision of the neural network are not the highest in each material classification, but the gap between the two is the smallest frequently. Thus, increasing both the precision and recall while minimizing the gap between the two is the direction to improve the classification accuracy of other classifiers.

With the same simulation data, the shape-based classification is analyzed, and the results are shown in Table 7 and Fig.13.

As shown in Fig.13, the accuracy of the classifiers is concentrated between 68%-90%. The neural network dis-

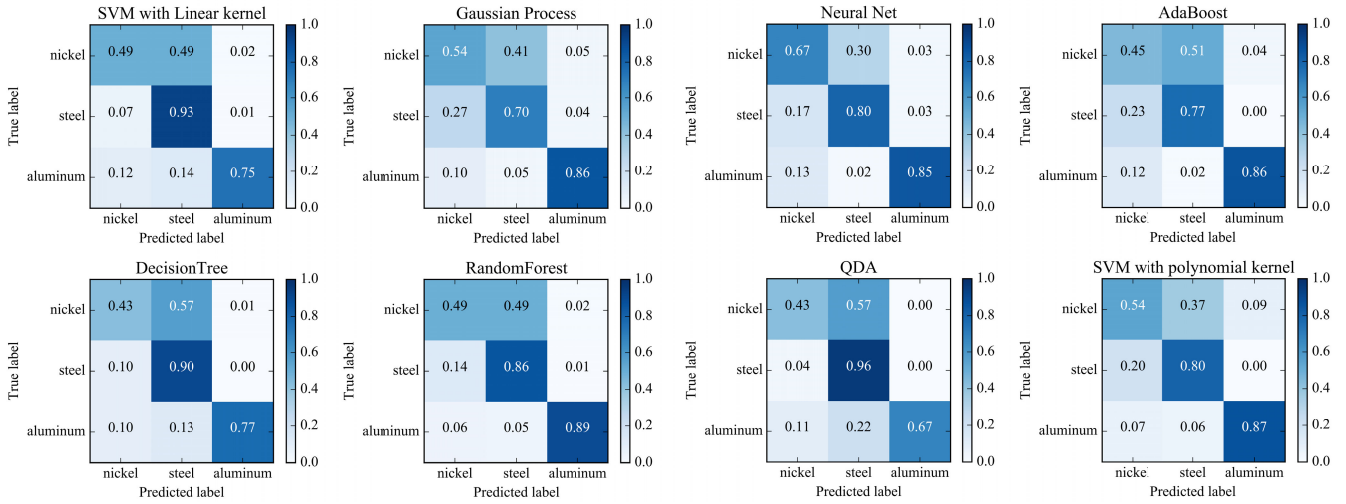

FIGURE 14. The results of material-based classification by confusion matrix.

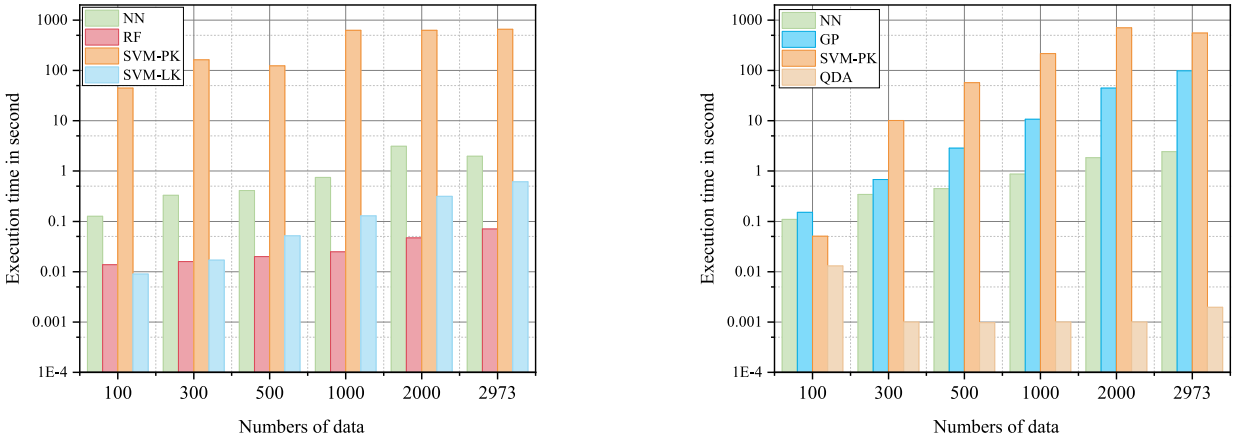

(a) material-based classification

(b) shape-based classification

FIGURE 15. Time complexity analysis of classification.

TABLE 7. precision and recall of shape-based classification.

Algorithm	a>b		a<b	
	precision	recall	precision	recall
SVM-LK	80.1%	62.2%	75.1%	88.1%
GP	87.3%	87.3%	90.2%	90.2%
DT	59.9%	68%	72.4%	64.9%
RF	64%	74.9%	77.7%	67.6%
NN	88.2%	86.9%	90%	91.1%
AdaBoost	73.1%	70.3%	77.7%	80.1%
QDA	83.5%	81.9%	86.2%	87.5%
SVM-PK	88.1%	85.7%	89.2%	91.1%

plays the highest classification accuracy among the eight classifiers. As shown in Table 7, regardless of the class of shape, the gap between the precision and the recall of most classifiers is relatively small. The classification accuracy of majority classifiers is higher than that of material-based classification, which verified the result in the sensitivity analysis of the spheroid model. SVM-LK has the problem of a relatively large gap between the recall and the precision in each shape classification, decision tree and random forest have the problem of lower values of both, which are the reasons for the poor accuracy of these three classifiers.

The above analysis of the classification algorithm by the accuracy, precision and recall mainly indicates the predictive capability of the algorithm in different classes. For shape-based classification, the classification performances are more excellent, and the labels are divided into two classes. Through the accuracy recall and precision, we have a thorough comprehension to the performance to various algorithms. But for material-based classification, since the labels are divided into three classes, there is no intuitive display of the class predicted by the classifier for the misclassified samples. Afterward, we evaluated the classification performances of material-based classification by confusion matrix.

Remarkably, the confusion matrix we implemented is a metric that improves on the basis of the classical confusion matrix. In the classical confusion matrix, the column labels represent the predicted labels, the row labels represent the true labels, and the diagonal elements represent the number of samples for which the predicted label is equal to the true label, which is not intuitive enough when the number of samples in each class imbalance. We call class imbalance when the number of samples in different classes is different. The elements of confusion matrix we implemented are normalized. For example, the elements on the diagonal represent the ratio of the samples predicted correctly to its true class. The situation of misclassification in each class is visually displayed. The diagonal value of confusion matrix is higher the performance is better, which indicates fewer incorrect predictions. The results of material-based classification are shown in Fig.14:

Among the eight classifiers, the classification performance of nickel is relatively poor. SVM with linear kernel, decision tree, random forest, adaboost, and QDA algorithm misclassify nearly half or even a larger proportion of nickel target as steel target. Even the best classifier, the neural network, misclassified 33% of the nickel target as steel. The classification performance of steel is relatively positive. The SVM with linear kernel, decision tree and QDA algorithm can achieve more than 90% classification accuracy for steel. Although other algorithms may misclassify the steel as nickel, the misclassify ratio is much smaller than that of nickel. The classification performance of aluminum is better. Most classifiers have a powerful ability to distinguish non-permeable materials from permeable materials, but QDA and SVM with linear kernel algorithms still misclassify a portion of aluminum into steel.

As shown in Fig.15,We performed the time complexity analysis for material-based classification and shape-based classification. We selected the four classifiers with the highest classification accuracy for time complexity analysis. We changed the size of the dataset to observe the execution time of different classifiers. All datasets of different size were randomly divided from the dataset. Due to the gap of each classifier's execution time is large, we chose the logarithmic axis to show the results.

In the time complexity analysis of material-based classification (Fig.15(a)), the execution time of each classifier increase with the size of dataset. It is worth noting that the execution time of SVM-PK is greatly affected by the size of datasets. In other words, when the data set is large, the execution time of SVM-PK is relatively long. However, when the data set is larger, the execution time of other three classifiers are less (within 4 seconds), and the classification accuracy of NN is the highest.

In the time complexity analysis of shape-based classification (Fig.15(b)), except for QDA, the execution time of each classifier increases with the size of dataset. Although the execution time of QDA is not sensitive to size of dataset, its classification accuracy is the lowest among the four classifiers. With the increase of dataset size, the execution time of SVM-PK and GP increases rapidly. As NN has the highest classification accuracy, the processing time of NN is within 3 seconds even when the size of dataset is large.

According to the evaluation results by common classification metrics (accuracy, recall, precision and confusion matrix) and time complexity, we can know that the performance of the neural network is the best in material-based classification and shape-based classification. For most classifiers, the result of shape-based classification is better than that of material-based classification. In future research, we need to optimize the parameters of the neural network algorithm to improve its performance on material-based classification, especially for nickel material classification.

VII. CONCLUSION AND FUTURE WORK

In this paper, we analyzed the factors that may affect the classification results in the classification process by performed sensitivity analysis on the model (spheroid model and the approximate forward model), analyzed the fitting algorithm and compared the classification results of eight classification algorithm. According to the sensitivity analysis of the spheroid model, the influence of the shape variable (radius R) on determining the output uncertainty was generally greater than that of the material variable (μ_r). The sensitivity analysis of the approximate forward model revealed that it is not feasible to classify objects when the orientation is unknown. To evaluating the influence of the fitting algorithm, we utilized the model parameters fitted from noise-added data sets as the classification attributes and compared the accuracy of eight classification algorithms in material-based classification and shape-based classification. We found that the results of the fitting algorithm are very sensitive to the noise level. By compared the classification performances of the eight classification algorithms in material-based classification and shape-based classification, it indicated that the performance of the neural network algorithm is better than other algorithms. When the data set at 30dB SNR is the training dataset, an accuracy of 89.2% was reported by using the NN algorithm in shape-based classification, an accuracy of 78.7% was reported by using the NN algorithm in material-based classification.

In the future work, first, we should get the target orientations before target classification. Second, it is necessary to improve the fitting algorithm performance so that it can still accurately fit model parameters in a noisy environment. Finally, we will improve classification algorithm performance on material-based classification. In particular, the parameters of the neural network algorithm should be optimized to improve its ability to distinguish permeable materials.

REFERENCES

[1] H. Widmer, M. Bittner, L. Sieber, and M. Fischer, "Systems, methods, and apparatus for detection of metal objects in a predetermined space," U.S. Patent 9 726 518, Aug. 8, 2017.

[2] S. Alahakoon, Y. Q. Sun, M. Spiryagin, and C. Cole, "Rail flaw detection technologies for safer, reliable transportation: A review," *J. Dyn. Syst., Meas., Control*, vol. 140, no. 2, 2018, Art. no. 020801.

[3] E. B. Banning, "The archaeological impacts of metal detecting," *Open Archaeol.*, vol. 5, no. 1, pp. 180–186, 2019.
[4] M. T. B. Tajudin, M. D. Ghazali, and M. K. S. Singh, "Patterns analysis of underground pipeline detection with different type of material and substance inside it by using ground penetrating radar (GPR)," in *Proc. Symp. Innov. Creativity (iMIT-SIC)*, vol. 3, 2017, pp. 1–4.
[5] H. Zhang, K. Yang, Z. Yang, P. Zhang, Y. Lu, and P. Yan, "Hyperspectral mineral mapping technology applied to geology based on HyMap data," *Proc. SPIE*, vol. 10156, Oct. 2016, Art. no. 101560Y.
[6] J. Willems, K. Ponsen, and B. Burger, "Metal implants and airport security checks," *Nederlands Tijdschrift Voor Geneeskunde*, vol. 162, Aug. 2018.
[7] H. W. Nørgaard, "Portable XRF on prehistoric bronze artefacts: Limitations and use for the detection of bronze age metal workshops," *Open Archaeol.*, vol. 3, no. 1, pp. 101–122, 2017.
[8] H. Kisanuki, K. Aoike, T. Ogahara, and T. Inazaki, "Detailed GPR survey for detecting boulders buried in a subgrade of a highway under construction," in *Proc. Symp. Appl. Geophys. Eng. Environ. Problems*, 2018, pp. 385–388.
[9] P. Zhang, X. Guo, N. Muhammat, and X. Wang, "Research on probing and predicting the diameter of an underground pipeline by GPR during an operation period," *Tunnelling Underground Space Technol.*, vol. 58, pp. 99–108, Sep. 2016.
[10] P. Xie, H. Wen, J. Fu, R. Li, and J. Hu, "A methodology for three dimensional modeling of subsurface geologic structure in mantled karst area," *J. Comput. Methods Sci. Eng.*, vol. 18, no. 3, pp. 667–682, 2018.
[11] U. Meyer, M. Frei, H. Petersen, A. Papenfuß, M. Ibs-Von Seht, R. Stolz, M. Queitsch, P. Buchholz, and B. Siemon, "HYPGEO—A collaboration between geophysics and remote sensing for mineral exploration," in *Proc. EGU General Assembly Conf. Abstracts*, vol. 19, 2017, p. 2442.
[12] P. Gao, C. Wang, Y. Li, and Z. Cong, "Electromagnetic and eddy current ndt in weld inspection: A review," *Insight-Non-Destructive Test. Condition Monitor.*, vol. 57, no. 6, pp. 337–345, 2015.
[13] S. D. Billings, L. R. Pasion, L. Beran, N. Lhomme, L.-P. Song, D. W. Oldenburg, K. Kingdon, D. Sinex, and J. Jacobson, "Unexploded ordnance discrimination using magnetic and electromagnetic sensors: Case study from a former military site," *Geophysics*, vol. 75, no. 3, pp. B103–B114, 2010.
[14] H. Ammari, J. Chen, Z. Chen, D. Volkov, and H. Wang, "Detection and classification from electromagnetic induction data," *J. Comput. Phys.*, vol. 301, pp. 201–217, Nov. 2015.
[15] R. Ward, M. Joseph, A. Langley, S. Taylor, and J. C. Watson, "Magnetic induction tomography of objects for security applications," *Proc. SPIE*, vol. 10438, Oct. 2017, Art. no. 104380G.
[16] A. Witten, *Handbook of Geophysics and Archaeology*. Evanston, IL, USA: Routledge, 2017.
[17] L. Qi, "Research on ground penetrating radar based on underground pipeline detection," *Building Technol. Develop.*, vol. 44, no. 14, p. 45, 2017.
[18] L. Ying, X. Hongyue, L. Qinmei, and J. Fan, "Application of electrical prospecting method in underground pipeline detection," *Geotechn. Invest. Surveying*, no. 5, p. 15, 2016.
[19] L. R. Pasion and D. W. Oldenburg, "Locating and determining dimensionality of UXOs using time domain electromagnetic induction," in *Proc. Symp. Appl. Geophys. Eng. Environ. Problems*, 1999, pp. 763–772.
[20] J. T. Smith, H. F. Morrison, and A. Becker, "Parametric forms and the inductive response of a permeable conducting sphere," *J. Environ. Eng. Geophys.*, vol. 9, no. 4, pp. 213–216, 2004.
[21] L. Pasion, L. Beran, K. Kingdon, and S. Billings, "Inversion and classification using the point dipole model: Practical experiences from munitions response demonstrations," in *Proc. SEG Annu. Meeting Soc. Explor. Geophys.*, 2011, pp. 3758–3762.
[22] L. C. Pi and L. Kennedy, "2009 ESTCP UXO discrimination study," ESTCP Program Office, Alexandria, VA, USA, Tech. Rep. MR-200501, 2009.
[23] D. A. Steinhurst, G. R. Harbaugh, J. B. Kingdon, T. Furuya, D. A. Keiswetter, and D. C. George, "EMI array for cued UXO discrimination," Environ. Secur. Technol. Certification Program, Alexandria, VA, USA, Tech. Rep. MM-0601, 2010.
[24] J. Makkonen, L. A. Marsh, J. Vihonen, A. Visa, A. Järvi, and A. J. Peyton, "Classification of metallic targets using a single frequency component of the magnetic polarisability tensor," *J. Phys., Conf. Ser.*, vol. 450, no. 1, 2013, Art. no. 012038.
[25] I. Shamatava, G. Schultz, and F. Shubitidze, "Accessing UXO classification technologies at a challenging live-UXO site," in *Proc. 48th Int. Seminar/Workshop Direct Inverse Problems Electromagn. Acoust. Wave Theory (DIPED)*, Sep. 2018, pp. 24–27.
[26] J. B. Sigman, Y. Wang, K. A. O'Neill, B. E. Barrowes, and F. Shubitidze, "An expert-free technique for live site UXO target classification," in *Proc. Symp. Appl. Geophys. Eng. Environ. Problems*. 2014, pp. 456–463.
[27] M. P. Bray and C. A. Link, "Learning machine identification of ferromagnetic UXO using magnetometry," *IEEE J. Sel. Topics Appl. Earth Observ. Remote Sens.*, vol. 8, no. 2, pp. 835–844, Feb. 2015.
[28] S. Lameri, F. Lombardi, P. Bestagini, M. Lualdi, and S. Tubaro, "Landmine detection from GPR data using convolutional neural networks," in *Proc. 25th Eur. Signal Process. Conf. (EUSIPCO)*, Aug./Sep. 2017, pp. 508–512.
[29] A. Bijamov, J. P. Fernández, B. E. Barrowes, I. Shamatava, K. O'Neill, and F. Shubitidze, "Camp Butner live-site UXO classification using hierarchical clustering and Gaussian mixture modeling," *IEEE Trans. Geosci. Remote Sens.*, vol. 52, no. 8, pp. 5218–5229, Aug. 2013.
[30] K. N. Kappler and E. Gasperikova, "A hybrid method for UXO vs. non-UXO discrimination," *J. Environ. Eng. Geophys.*, vol. 16, no. 4, pp. 177–189, 2011.
[31] I. Mitiche, M. D. Jenkins, P. Boreham, A. Nesbitt, B. G. Stewart, and G. Morison, "Deep residual neural network for EMI event classification using bispectrum representations," in *Proc. 26th Eur.Signal Process. Conf. (EUSIPCO)*, Sep. 2018, pp. 186–190.
[32] S. N. A. M. Kanafiah, A. A. Firdaus, N. F. Jefri, N. N. Karim, N. S. Khalid, I. I. Ismail, M. J. M. Ridzuan, M. A. Ismail, and M. R. Ahmad, "Fundamental shape discrimination of underground metal object through one-axis ground penetrating radar (GPR) scan," *J. Telecommun., Electron. Comput. Eng.*, vol. 10, nos. 1–13, pp. 43–47, 2018.
[33] L. Beran and D. W. Oldenburg, "Selecting a discrimination algorithm for unexploded ordnance remediation," *IEEE Trans. Geosci. Remote Sens.*, vol. 46, no. 9, pp. 2547–2557, Sep. 2008.
[34] L. R. Pasion, "Inversion of time domain electromagnetic data for the detection of unexploded ordnance," Ph.D. dissertation, Dept. Graduate Stud., Univ. Brit. Columbia, Vancouver, BC, Canada, 2007.
[35] D. Keiswetter, "Advanced signal processing & classification: UXO standardized test site data," Sci. Appl. Int. Corp, San Diego, CA, USA, Tech. Rep. MR-1505, 2012.
[36] L. R. Pasion, S. D. Billings, D. W. Oldenburg, and S. E. Walker, "Application of a library based method to time domain electromagnetic data for the identification of unexploded ordnance," *J. Appl. Geophys.*, vol. 61, nos. 3–4, pp. 279–291, 2007.
[37] J. T. Smith and H. F. Morrison, "Approximating spheroid inductive responses using spheres," *Geophysics*, vol. 71, no. 2, pp. G21–G25, 2006.
[38] C. P. Oden, "Combining advances in EM induction instrumentation and inversion schemes for UXO characterization," *Prog. Electromagn. Res. B*, vol. 38, pp. 107–134, Jan. 2012.
[39] F. Weber, S. Theers, D. Surmann, U. Ligges, and C. Weihs, "Sensitivity analysis of ordinary differential equation models," Tech. Rep., 2018.
[40] P. Lison, "An introduction to machine learning," to be published.
[41] A. Singh, N. Thakur, and A. Sharma, "A review of supervised machine learning algorithms," in *Proc. 3rd Int. Conf. Comput. Sustain. Global Develop. (INDIACom)*, Mar. 2016, pp. 1310–1315.
[42] X. Zhu, "Semi-supervised learning," in *Encyclopedia of Machine Learning and Data Mining*. 2017, pp. 1142–1147.
[43] C. Xu, D. Chai, J. He, X. Zhang, and S. Duan, "InnoHAR: A deep neural network for complex human activity recognition," *IEEE Access*, vol. 7, pp. 9893–9902, 2019.
[44] B. Hammer, D. Nebel, M. Riedel, and T. Villmann, "Generative versus discriminative prototype based classification," in *Advances in Self-Organizing Maps and Learning Vector Quantization*. Berlin, Germany: Springer, 2014, pp. 123–132.
[45] T. Cacoullos, Ed., *Discriminant Analysis and Applications*. New York, NY, USA: Academic, 2014.
[46] J. Hensman, A. Matthews, and Z. Ghahramani, "Scalable variational Gaussian process classification," 2015, *arXiv:1411.2005*. [Online]. Available: https://arxiv.org/abs/1411.2005
[47] B. Hssina, A. Merbouha, H. Ezzikouri, and M. Erritali, "A comparative study of decision tree ID3 and C4.5," *Int. J. Adv. Comput. Sci. Appl.*, vol. 4, no. 2, pp. 1–7, 2014.
[48] L. Breiman, *Classification and Regression Trees*. Evanston, IL, USA: Routledge, 2017.
[49] G. Louppe, "Understanding random forests: From theory to practice," 2014, *arXiv:1407.7502*. [Online]. Available: https://arxiv.org/abs/1407.7502
[50] G. Haixiang, L. Yijing, L. Yanan, L. Jinlinga, and L. Xiao, "BPSO-Adaboost-KNN ensemble learning algorithm for multi-class imbalanced data classification," *Eng. Appl. Artif. Intell.*, vol. 49, pp. 176–193, Mar. 2016.

[51] W. Al-Salman, Y. Li, P. Wen, and M. Diykh, "An efficient approach for EEG sleep spindles detection based on fractal dimension coupled with time frequency image," *Biomed. Signal Process. Control*, vol. 41, pp. 210–221, Mar. 2018.
[52] M. van Gerven and S. Bohte, *Artificial Neural Networks as Models of Neural Information Processing*. Lausanne, Switzerland: Frontiers Media SA, 2018.
[53] D. P. Kingma and J. Ba, "Adam: A method for stochastic optimization," 2014, *arXiv:1412.6980*. [Online]. Available: https://arxiv.org/abs/1412.6980
[54] K. M. Ting, "Confusion matrix," in *Encyclopedia of Machine Learning and Data Mining*. Ithaca, NY, USA: Cornell Univ., 2017, p. 260.
[55] W. Al-Salman, Y. Li, and P. Wen, "Detecting sleep spindles in EEGs using wavelet Fourier analysis and statistical features," *Biomed. Signal Process. Control*, vol. 48, pp. 80–92, Feb. 2019.
[56] T. M. Grzegorczyk and B. E. Barrowes, "Real-time processing of electromagnetic induction dynamic data using Kalman filters for unexploded ordnance detection," *IEEE Trans. Geosci. Remote Sens.*, vol. 51, no. 6, pp. 3439–3451, Jun. 2013.
[57] D. Ambruš, D. Vasić, and V. Bilas, "Robust estimation of metal target shape using time-domain electromagnetic induction data," *IEEE Trans. Instrum. Meas.*, vol. 65, no. 4, pp. 795–807, Apr. 2016.
[58] T. M. Grzegorczyk, B. E. Barrowes, F. Shubitidze, J. P. Fernandez, and K. O'Neill, "Simultaneous identification of multiple unexploded ordnance using electromagnetic induction sensors," *IEEE Trans. Geosci. Remote Sens.*, vol. 49, no. 7, pp. 2507–2517, Jul. 2011.

SHIHONG DUAN received the B.E. and Ph.D. degrees in pattern recognition and computer science from the University of Science and Technology Beijing (USTB), China, in 1998 and 2012, respectively. Since July 2013, she has been an Associate Professor with the School of Computer and Communication Engineering, USTB, where she was an Assistant Professor, from January 1998 to June 2013. From August 2014 to August 2015, she was a Visiting Scholar with the Center for Wireless Information Network Studies, Department of Electrical and Computer Engineering, Worcester Polytechnic Institute. Her research interests include wireless channel study, human activity recognition, mobile robotics, and underground target detection.

YUE LI received the B.E. degree from the Industrial and Commercial College, Hebei University, in 2016. She is currently pursuing the master's degree with the School of Computer and Communication Engineering, University of Science and Technology Beijing, China. Her current research interest includes underground target classification.

YADONG WAN received the B.E. and Ph.D. degrees from the University of Science and Technology Beijing, in 2003 and 2010, respectively. He was a Visiting Scholar in wireless location with the Worcester Polytechnic Institute, from August 2012 to February 2013. His current research interests include underground target detection, industrial wireless sensor networks, signal processing, and data science of materials genome initiative.

PENG WANG received the B.E. and Ph.D. degrees from the University of Science and Technology Beijing, in 2012 and 2018, respectively. His current research interests include underground target detection, low frequency wireless communication, wireless sensor networks, adaptive signal processing, and near field electromagnetic localization.

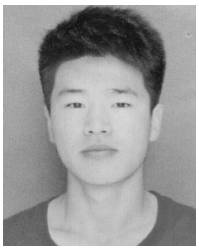

ZHEN WANG received the B.E. degree from the North China Institute of Aerospace Engineering, in 2018. He is currently pursuing the master's degree with the School of Computer and Communication Engineering, University of Science and Technology Beijing, China. His current research interest includes underground target detection.

NA LI received the B.E. and M.S. degrees from the University of Science and Technology Beijing, China, in 2001 and 2006, respectively, where she has been beginning to work, since 2006. Her current research interests include multivariate statistical analysis, statistical learning theory, and machine learning.